Article

Machine learning based cellular contractile force detection: a new approach to predict cell mechanics by images

Honghan Li[1], Daiki Matsunaga[1,*], Tsubasa S. Matsui[1], Hiroki Aosaki[1], Koki Inoue[1], Amin Doostmohammadi[2], and Shinji Deguchi[1,*]

[1]Division of Bioengineering, Graduate School of Engineering Science, Osaka University, 1-3 Machikaneyama Toyonaka, Osaka, 5608531, Japan
[2]Niels Bohr Institute, University of Copenhagen, Blegdamsvej 17, 2100 Copenhagen, Denmark
[*]Correspondence: daiki.matsunaga@me.es.osaka-u.ac.jp, deguchi@me.es.osaka-u.ac.jp

ABSTRACT In this paper, we propose a new machine learning system that can predict the cellular force distributions from the microscope images. The full process can be divided into three steps. First, we culture the cells on a special substrate and measure both the cellular contractile force and the substrate wrinkles simultaneously. The cellular contractile forces are obtained using the traction force microscopy (TFM), while cells generate wrinkles thanks to our original plasma-irradiated substrates. Second, the wrinkle positions are extracted from the microscope images by using SW-UNet. Third, we train the machine learning system with GAN (generative adversarial network) by using sets of corresponding two images, the force distributions and the input images (raw microscope images or extracted wrinkle images), as the training data. The network understands the way to convert the input images to the force distributions from the training. After sufficient training, the network can be utilized to predict the cellular forces just from the input images. Comparing with the TFM experiment (test data), our system has 33-35% errors in the force magnitude prediction and angle errors 19-20° in the force direction. The system would be a powerful tool to evaluate the cellular forces efficiently because the forces can be predicted just by observing the cells, which is a way simpler method compared to the TFM experiment. We believe that our machine learning based system will be an useful method for other cellular assay applicants and researches in the future.

INTRODUCTION

Proliferative cells sense mechanical cues in the surrounding microenvironment to regulate their functions on the proliferation, differentiation, apoptosis, and pro-inflammation (1). Many of the mechanical cues are converted into a level of cellular inherent contractility or traction forces and in turn into intracellular signals regulating the related functions(2, 3). Traction forces, thus related to various cell functions, are generated by the activity of nonmuscle myosin II and actin (4, 5). Because these proteins work downstream of diverse signaling pathways, it is often difficult to predict how the force may change upon perturbations to particular molecules such as gene mutations and drug administration. Thus, technologies allowing for efficiently evaluating the cellular traction force are expected to appear to enhance comprehensive understanding of the force-related pathways.

We previously developed a wrinkle assay, a modified version of the method originally reported by Harris and colleagues (6, 7), in which the silicone substrates are spatially uniformly treated with oxygen plasma to allow them to buckle upon the forces exerted by cells (8–10). As the individual wrinkles are lengthened with the increase in the forces (11), the wrinkle length detected by a machine learning(12) can be used as a measure of the relative change in the force caused by perturbations such as specific gene mutations. While this technology is promising in that these experiments are performed easily to potentially enable a high-throughput analysis on the force-related pathways, the interpretation of the wrinkle length was not necessarily straightforward to be exact in terms of mechanics.

To overcome this limitation in quantification, here we describe a new machine learning system that converts the wrinkle information taken by a microscope into the actual cellular force distributions. The cellular contractile forces are obtained using the traction force microscopy (TFM), and we train the machine learning system with GAN (generative adversarial network) so that the network understands the way to convert the input microscope images to the force distributions from the training data. After sufficient training, the network can be utilized to predict the cellular forces just from the input images. The system would be a powerful tool to evaluate the cellular forces efficiently because the forces can be predicted just by observing the cells, which is a way simpler method compared to the TFM experiment.

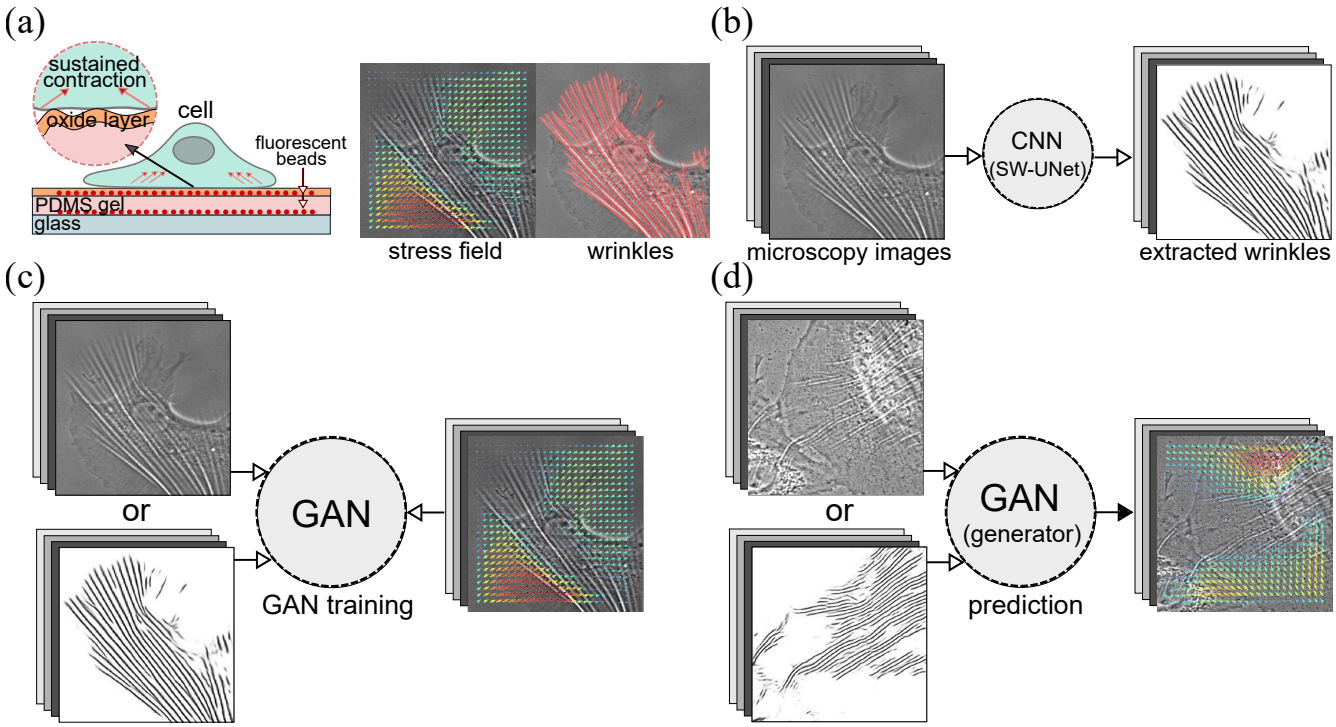

Figure 1: Overview of the methods and procedures that are utilized in the current paper. (a) Schematic of our experimental setup. A special substrate, which can evaluate the cellular force distribution (obtained by traction force microscopy) and the surface wrinkles simultaneously, is utilized in this work. (b) The surface wrinkles are extracted from the microscope images by using our machine learning system (SW-UNet). (c) The machine learning system (GAN) is trained to understand the relation between the input images (raw microscope image, or extracted wrinkle images) and corresponding output images (cellular force distribution). (d) After sufficient training, the system can predict the force distributions just by the microscope images.

MATERIALS AND METHODS

Overview

Figure 1 summarize the full picture of the current paper, and our goal is to construct a machine learning system that can predict the cellular force distributions from the microscope image or the extracted substrate wrinkles. The full process can be divided into three steps as shown in Fig. 1. First, we culture the cells (A7r5; embryonic rat vascular smooth muscle cells) on a special substrate and measure both the cellular contractile force and the substrate wrinkles simultaneously. As shown in Fig. 1(a), the cellular contractile forces are obtained using the traction force microscopy (TFM) (13), and cells generate wrinkles because the surface of PDMS layer is harden by the plasma irradiation (9, 12, 14–16). Second, the wrinkle positions are extracted from the microscope images as shown in Fig. 1(b) by using our SW-UNet (12), which is a CNN that reflects the concept of the small networks (17, 18). Third, the machine learning system utilizing GAN (19) is trained to understand a way to convert the microscope image, or the extracted wrinkle image to the cellular force distributions as shown in Fig. 1(c).

After the training, the network can be utilized to predict the cellular forces just from the microscope images. As also explained in the introduction, the system would be a powerful tool to evaluate the cellular forces efficiently because the forces can be predicted just by inputting the microscope images to our system, which is a way simpler method compared to the TFM experiments. In following subsections, we report each procedure in details.

Substrate preparation

Based on our previous studies (9, 12, 14–16), we prepared the substrate that can reversibly generate wrinkles upon application of cellular forces. Firstly, parts A and B of CY 52-276 (Dow Corning Toray) are mixed at a weight ratio of 1.2:1 to form a PDMS (polydimethylsiloxane) gel layer that is coated on a circular cover glass. Secondly, the cover glass is placed in a 60°C oven for 20 hours to cure the PDMS gel. Thirdly, oxygen plasma (SEDE-GE, Meiwafosis) is applied uniformly along the surface of the PDMS layer to create an oxide layer that works as the substrate for cell culture. Finally, the substrate is coated with 10

μg/mL collagen type I solution for 3 hours.

For the TFM measurement, fluorescent micro-beads are attached to the substrate surface as position markers to measure the substrate deformations. The beads need to be firmly adhered to the surface so that cells would not move the beads due to cytosis. In this work, the covalent bonding between the surface and beads are realized by following two steps; (i) silane coupling of the substrate surface and (ii) the covalent bonding formation due to carbodiimide. The beads are also placed on the cover glass and adhered by the covalent bonding as shown in Fig.1(a) to keep the reference position even after removing the cell using 0.25% or 0.05% Trypsin (Trypsin + 1mm mol/l EDTA 4Na solution; Fuji Wako Pure Chemical Corporation).

Cell culture and microscope setup

A7r5 (embryonic rat vascular smooth muscle cells) cells were maintained in a stage incubator (INUF-IX3W; Tokai Hit) under a humidified 5% CO_2 incubator at 37°C. An inverted microscope (1X73; Olympus Corporation) with a conforcal unit (CSU10; Yokokawa Electric) and oil immersion lens (phase contrast, UPlanFLN 60x/1.25 Oil Iris Ph3, Olympus Corporation) are used to capture the cells. During the experiment, DMEM(L)+10% FBS+Penicillin-Streptomycin (Fuji Wako Pure Chemical Corporation) is used as the culture medium.

Traction force microscopy (TFM)

The software ImageJ/Fiji and its plugin FTTC (Fourier transform traction cytometry) (20, 21) is used to evaluate the contractile force displacement from the displacement field. The substrate is considered as a soft elastic isotropic material that follows the linear elastic theory. First, the displacement of the substrate surface $\boldsymbol{u}$ is measured by tracking the movement of the fluorescent beads using PIV (particle image velocimetry). Second, the stress field is obtained from the displacement field by solving the governing equation for the elastic halfspace (22, 23) given by

$$\boldsymbol{u}(\boldsymbol{x}) = \int_S \boldsymbol{G}(\boldsymbol{x},\boldsymbol{y})\boldsymbol{t}(\boldsymbol{y})dS(\boldsymbol{y}) \tag{1}$$

where $\boldsymbol{t}$ is the traction force, $\boldsymbol{x}$ and $\boldsymbol{y}$ are the positions of the displacement and the traction force, respectively. $\boldsymbol{G}$ is the Green's function that is given by

$$\boldsymbol{G}(\boldsymbol{x}) = \frac{1+\nu}{\pi E r^3}\begin{pmatrix}(1-\nu)r^2+\nu r_x^2 & \nu r_x r_y \\ \nu r_x r_y & (1-\nu)r^2+\nu r_y^2\end{pmatrix} \tag{2}$$

where E is the Young's modulus, ν is the Poisson's ratio, $\boldsymbol{r} = (r_x, r_y) = \boldsymbol{x} - \boldsymbol{y}$ is the relative vector and $r = |\boldsymbol{r}|$. The software FFTC solves Eq. (1) in the Fourier space, which is given by

$$\tilde{\boldsymbol{t}} = (\boldsymbol{G}^T\boldsymbol{G} + \lambda^2\boldsymbol{I})^{-1}\boldsymbol{G}^T\tilde{\boldsymbol{u}} \tag{3}$$

where tilde symbols denote that the variables in Fourier space, λ is the regularization parameter (23) and $\boldsymbol{I}$ is the unit tensor. In order to evaluate the optimal parameter λ for the Tikhonov regularization, the L-curve criterion (23, 24) is applied. Note that parameters $E = 5400$ Pa and $\nu = 0.5$ (incompressible) are used in the force estimation.

Wrinkle extraction

We use a new method SW-UNet (12), which is a CNN that based on U-Net (25) to extract wrinkle patterns from the microscope image as shown in Fig. 1(b). As the training data, we prepare 236 sets of corresponding two images (microscope image and manually labeled wrinkle image). The number of data is increased to 2596 by using the image augmentation techniques. We used NVIDIA Titan RTX to accelerate the training process, and the Adam optimizer is utilized.

Preparation of training data

Assume that we have N_o sets of corresponding images and data; the input images x (microscope images, or extracted wrinkle images) and the force distributions y as shown in Fig. 2. We effectively have the number of training data set $2N_o$ because the wrinkle image has only 1D information at each pixel (intensity $I(x, y)$; see also images in Fig. 2) while the force distributions have 2D information (2D force, $\boldsymbol{f}(x, y) = \{f_x(x, y), f_y(x, y)\}$). We designed the network to evaluate the cellular force only for a single axis at one time and focus only on the x-directional force at each evaluation. An input image I_i is used as the training data set (I_i, f_x) and (I_i', f_y) where I_i' is an image that rotate I_i by 90 degree.

The force distributions are converted to gray scale images that have intensities

$$I(f_d) = a \arctan\left(\frac{f_d}{b}\right) + I_{\mathrm{mid}} \tag{4}$$

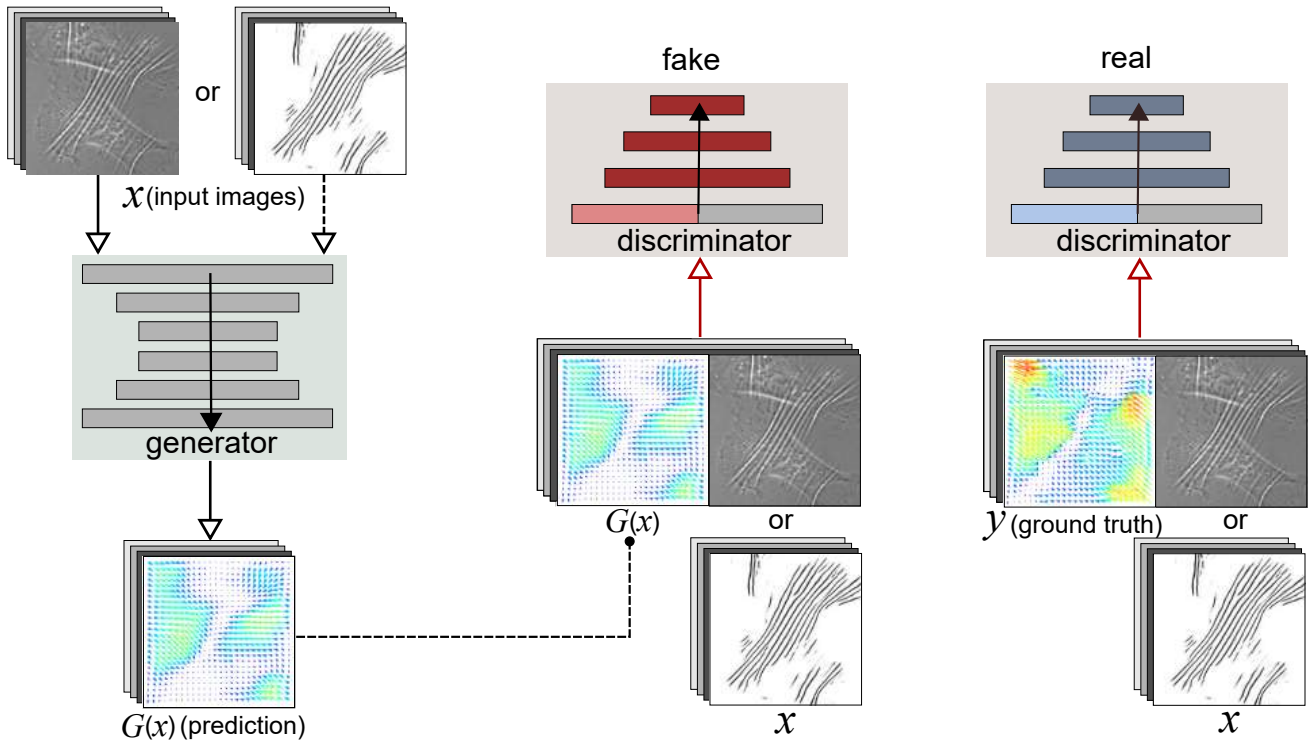

Figure 2: Schematic showing the structure of GAN (generative adversarial network) utilized in the present work.

where $a = 81.2$, $b = 50.0$, $I_{\mathrm{mid}} = 255/2$ are the coefficients for the conversions, and f_d is the components of the force $d = x, y$. The force distributions in gray scale, which are generated from the test images, can be converted back to the force using this equation. As the training data, we prepared $N = 332$ sets (83 original images) of corresponding two images. Note that we increased the number of training data by rotating the images, $83 \times 4 = 332$.

GAN structure

Our goal is to convert the a physical quantity (wrinkle geometry) to the other physical quantity (force distribution). Even though the mechanical formulation between the two quantity is given, it is not necessarily straightforward to solve this inverse problem because of its complex nonlinear dynamics (26, 27). Instead, we achieve this purpose by training our machine learning system to understand the underlying mechanical rules. Considering this conversion of the physical quantity as a the image "translation", we utilize GAN (generative adversarial network) (28) in this work.

GAN mainly consists of two networks, generator G and discriminator D as shown in Fig. 2, and the network is trained by a competition of two networks. Goal of the generator G is to generate fake images (fake force distributions $G(x)$) from the input images x (microscope images or extracted wrinkle images) and tries to mimic the real images y (real force distributions), while the discriminator D tries to distinguish true and fake images from the group of images. As the training proceed, the generator learns how to produce fake images that are difficult to be distinguished by the discriminator from the real images, and the discriminator learns the rules to distinguish true/fake images. Once the training completes, the trained generator G can be used as the translator to predict the force distribution from the input images x even for test images, which were not including in the training process.

In present work, we design the generator G with a form of encoder-decoder which based on U-Net (25) but without the copy-and-crop path, and Markovian discriminator (PatchGAN) (29) is utilized as the discriminator D. The generator G converts the input image x to the fake force distribution images $G(x)$. The images of force distribution, y or $G(x)$, and the input images x are concatenated into a single image as the input of discriminator. The two networks G and D are trained based on the labels of real/fake, and we utilize the loss function $\mathcal{L}$ that is used in pix2pix (19):

$$\mathcal{L}(G, D) = \mathbb{E}_{x,y}[\log D(x, y)] + \mathbb{E}_x[\log(1 - D(x, G(x)))] + \lambda L_1(y, G(x)) \tag{5}$$

where $\mathbb{E}$ is the expected value, $L_1(G)$ is the L1 distance between generated images $G(x)$ and ground truths y and $\lambda = 100$ is the weight for the L1 term. The first term $\mathbb{E}[\log D]$ denotes the expected probability that the discriminator categorize y as the real

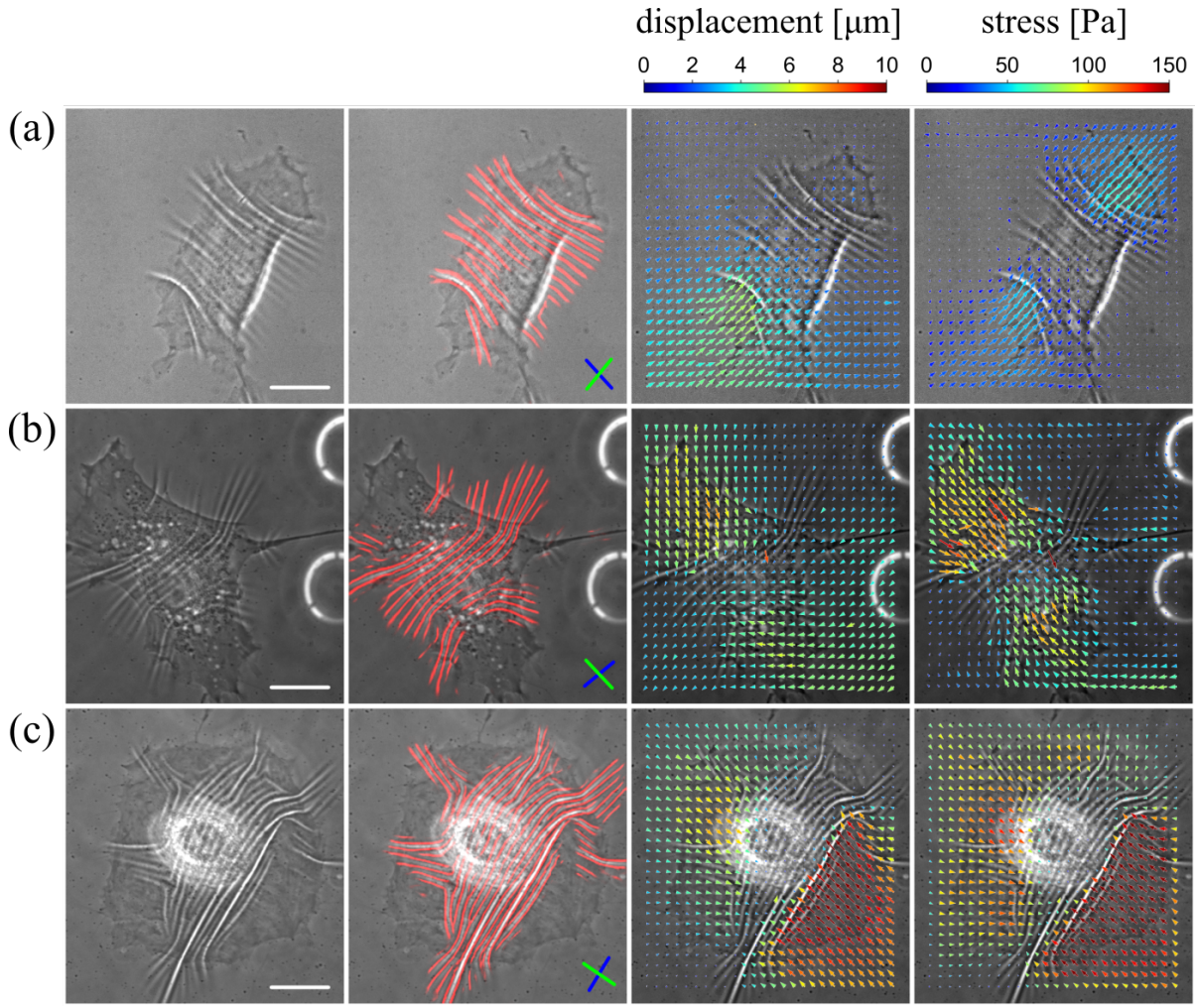

Figure 3: Three examples of the simultaneous measurement of wrinkles and traction forces. Each column describes (from left to right) raw image, wrinkles (red lines), displacement field and traction force field. The white scale bar in the first column images is 20 μm. The blue and green lines inside the second column images describe the principal direction of the wrinkle and the stress tensor, respectively.

data, while the second term $\mathbb{E}[\log(1 - D(x, G(x)))]$ denotes the probability that the discriminator categorize the generated image $G(x)$ as the fake data. The goal of the generator G is to minimize $\mathcal{L}$ while the discriminator D tries to maximize.

We use the training parameters as follow: 100 training epochs (batch size = 1), $\varepsilon = 0.0002$ learning rate for generator and discriminator, the parameters $\beta_1 = 0.5$ and $\beta_2 = 0.9$ are used for the Adam optimizer. The whole learning process is again accelerated by Nvidia Titan RTX.

RESULTS

Simultaneous measurement of wrinkles and traction forces

Figure 3 summarizes the result obtained by the experiment. Due to the pairwise cellular contractile force (fourth column), the substrates exhibit displacements toward the cell center (third column). As the result of the contraction, the wrinkles emerge mostly underneath the cells (second column). The wrinkles are aligned in a same direction as Fig. 3(a) when the cell size is small, while they tend to point multiple directions when the cell size is large and the contraction force is strong as Fig. 3(c).

Figure 4(a) shows the probability distribution function (PDF) of the stress magnitude of $N \times M$ samples, where $N = 103$ is the number of the images and $M = 26 \times 26$ is the number of the force observation points. The averages force is 50.3 ± 57.1 [Pa]. Figure 4(b) shows that the wrinkle length has a positive correlation with the mean traction force of the image, which is in

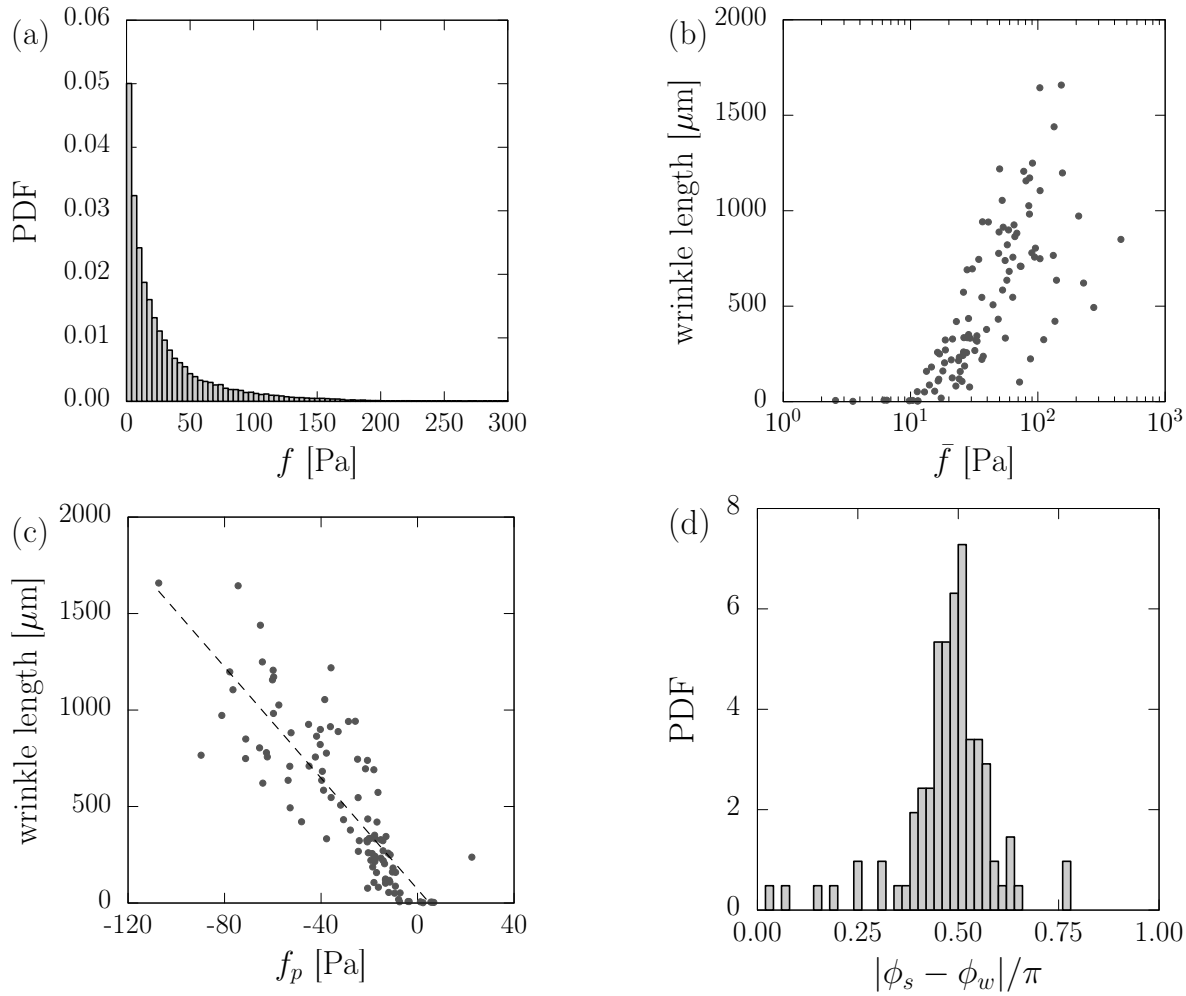

Figure 4: (a) Probability distribution function (PDF) of the stress magnitude. (b) The wrinkle length as the function of the mean force $\bar{f}$. Note that the wrinkle length is evaluated by counting the number of pixels after skeletonizing the wrinkle images. (c) The wrinkle length as the function of the principal force f_p. (d) Probability distribution function of the angle differences between direction of the wrinkles ϕ_w and the stress direction ϕ_s. The figure suggests that the direction of the wrinkles are perpendicular to the principal direction of the force most of the time.

agreement with our previous study (14). The mean force is simply obtained by averaging the norm of the force of the image as

$$\bar{f} = \frac{1}{M}\sum_{m}^{M} |\boldsymbol{f}_m| \tag{6}$$

where m is the index of the observation point. The wrinkle length is measured by counting the number of pixels after skeletonizing the wrinkle images (14). The wrinkle extincts when the mean force in a image is less than 10 Pa.

In order to analyze the principal direction of the stress, we construct a symmetric stress tensor for each image as

$$S_{ij} = \frac{1}{2M}\sum_{m}^{M} \left\{ n_j(\boldsymbol{x}_m, \boldsymbol{x}_0) f_i(\boldsymbol{x}_m) + n_i(\boldsymbol{x}_m, \boldsymbol{x}_0) f_j(\boldsymbol{x}_m) \right\} \tag{7}$$

where $\boldsymbol{r} = \boldsymbol{x}_m - \boldsymbol{x}_0$ is the relative vector from the image center $\boldsymbol{x}_0$ and $\boldsymbol{n} = \boldsymbol{r}/|\boldsymbol{r}|$ is the normal vector. By diagonolizing the tensor, we obtain the principal direction of the stress ϕ_s (shown in Fig. 3, second column with green lines) together with the corresponding principal force magnitude f_p, from the eigenvalue that has the largest norm. At the same time, we obtain the principal direction of the wrinkles ϕ_w (also shown in Fig. 3, second column with blue lines) from the 2D-FFT (fast Fourier

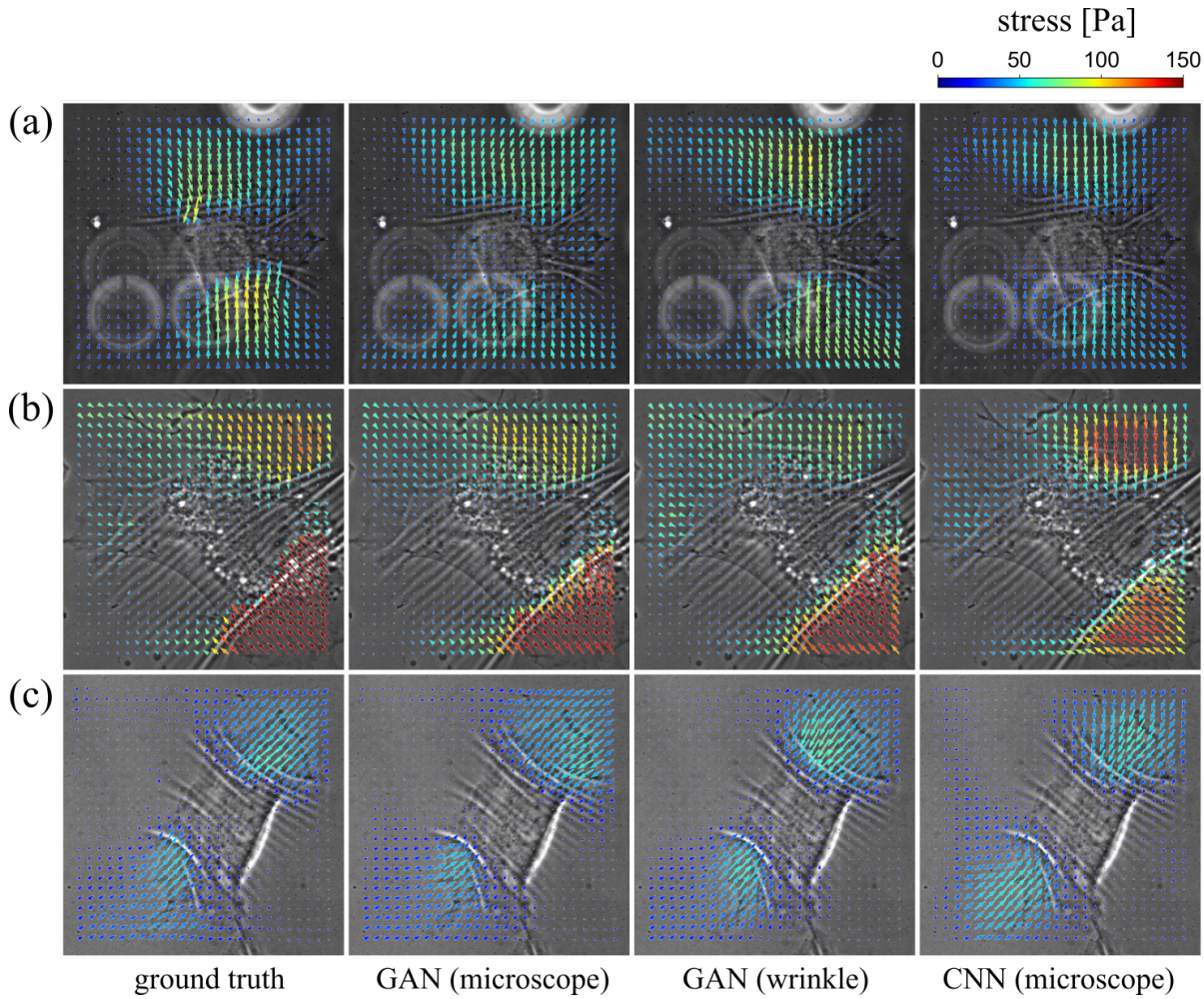

Figure 5: Prediction of the contractile forces. Each column shows the result of the contractile force by using different methods (from left to right): ground truth, GAN prediction (input: microscope image), GAN prediction (input: extracted wrinkle images), and CNN prediction (input: microscope image).

transform) image of the wrinkles: ϕ_w is an angle that is perpendicular to the direction that has a largest power spectrum. Figure 4(c) shows that the traction force is contractile ($f_p < 0$) and has almost linear relation (correlation $R = -0.82$ in a range $f_p < -5$ Pa) with the wrinkle length. Using the relation between the force and the wrinkles, the wrinkles can be used for one qualitative marker or indicator for rough estimation in the cellular force magnitude. Figure 4(d) shows that the two angles ϕ_s and ϕ_w are perpendicular most of the time. Since the wrinkle direction is perpendicular to that of the force dipoles, the wrinkle would be also practical to predict the force directions.

Traction force prediction using GAN

Finally, we train the network and evaluate the performance of the force estimation using our GAN network. Figure 5 compares the predicted force distributions which where estimated by three different methods. As also shown in Fig. 2, we trained the network with two different input images, the raw microscope images (second column in Fig. 5) and the extracted wrinkle images (third column), to compare the performances. We also evaluated the force distribution using a standard encoder-decoder type CNN and show the results in the fourth column. The figure shows that all three methods reproduce approximately the same force direction as the ground truth (first column), and the forces are perpendicular to the wrinkles.

In order to quantify the error in the force estimation, we introduce two errors: the error in the force amplitude ε_f and the force direction ε_θ. The error ε_f is defined to evaluate the difference in the force amplitude between the ground truth f^{true} and

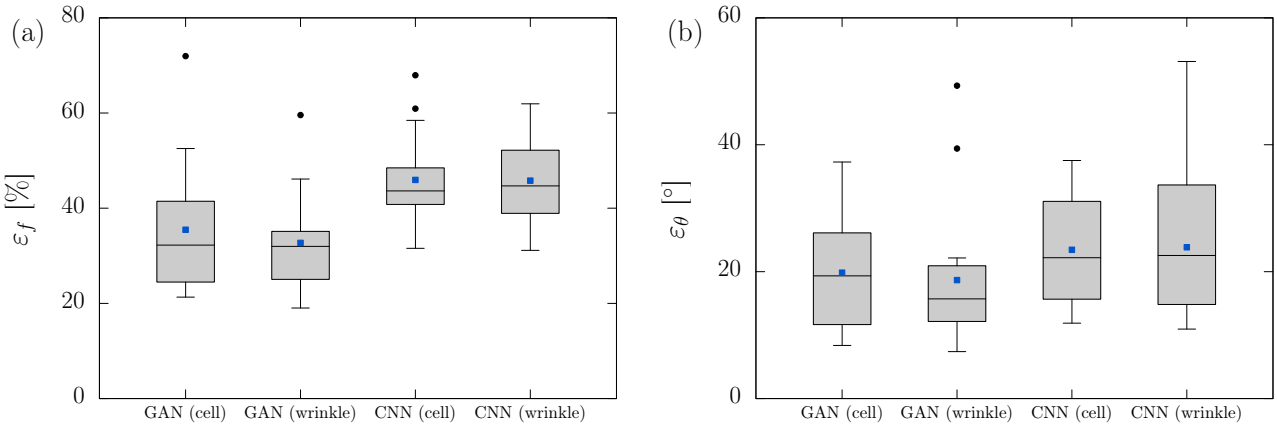

Figure 6: Errors of the predicted force compared to the ground truth data: (a) error in the force amplitude ε_f and (b) the force direction ε_θ. Blue squares are the average value and black circles denote the outliers.

the prediction f^{predict} as:

$$\varepsilon_f = \frac{1}{M}\sum_{m}^{M} \frac{|f_m^{\text{predict}} - f_m^{\text{true}}|}{f_m^{\text{true}}} \cdot \omega_m \tag{8}$$

where $M = 26 \times 26$ is the number of observation points, $\omega_m = f_m^{\text{true}}/\bar{f}$ is the weight function and $\bar{f}$ is the average force in a image which is defined in Eq. (6). Note that we introduce this weight function in order to put weight on the evaluation of large vectors rather than small vectors, which give huge errors even for small differences. We used $N = 332$ training images sets and 3 test images for the evaluation. The total error is calculated by averaging the error of 15 test images, which are obtained by repeating the evaluation 5 times with randomly selected different test images. Figure 6(a) shows that the error is 33-35% for GAN, and it has better performance compared to the encoder-decoder type simple CNN. There are no significant difference by the two input images, and this result indicates that performance of the force estimation would not improve drastically by explicitly teaching the wrinkle position to the machine learning system. Next, we evaluate the angle difference between the forces as

$$\varepsilon_\theta = \frac{1}{M}\sum_{i}^{M} |\theta_m^{\text{predict}} - \theta_m^{\text{true}}| \cdot \omega_m \tag{9}$$

where $\theta = \arctan(f_y/f_x)$ is the force direction. Figure 6(b) shows that the errors are 19-20° for GAN, and again shows better performance compared to conventional CNN. As for a traditional CNN, the loss function is designed to measure the error between predicted results and ground truth, and this criteria of the error is fixed during the training. While in the case of GAN, the loss function can adapt to the specific problem dynamically because of the discriminator network, and this difference brings GAN a better score as show in the figure.

In conclusion, our system succeeded in estimating the force distribution just from the input images with fairly small errors. The system would be a powerful tool to evaluate the cellular forces efficiently because the forces can be predicted just by observing the cells, which is a way simpler method compared to the TFM experiment.

DISCUSSION AND CONCLUSION

In this paper, we proposed a new machine learning system that can predict the cellular force distributions from the microscope images. The full process can be divided into three steps. First, we culture the cells on a special substrate and measure both the cellular contractile force and the substrate wrinkles simultaneously. The cellular contractile forces are obtained using the traction force microscopy (TFM), while cells generate wrinkles thanks to our original plasma-irradiated substrates. Second, the wrinkle positions are extracted from the microscope images by using SW-UNet. Third, we train the GAN system by using sets of corresponding two images, the force distributions and the input images (raw microscope images or extracted wrinkle images), as the training data. The network understands the way to convert the input images to the force distributions from the training. After sufficient training, the network can be utilized to predict the cellular forces just from the input images. Comparing with the TFM experiment (test data), our system has 33-35% errors in the force magnitude prediction and angle errors 19-20° in the force direction. The system would be a powerful tool to evaluate the cellular forces efficiently because the forces can be

predicted just by observing the cells, which is a way simpler method compared to the TFM experiment. We believe that our machine learning based system will be an useful method for other cellular assay applicants and researches in the future.

AUTHOR CONTRIBUTIONS

H.L., K.I. and D.M. developed the machine learning system. H.A. and T.S.M. designed and worked on the cell experiments. H.L., H.A. and D.M. analyzed the experimental data. A.D. and D.M. analyzed the physics. H.L., D.M. and S.D. wrote the article and designed the research.

ACKNOWLEDGMENTS

REFERENCES

1. Engler, A. J., S. Sen, H. L. Sweeney, and D. E. Discher, 2006. Matrix elasticity directs stem cell lineage specification. *Cell* 126:677–689.

2. Wang, N., I. M. Tolic-Nørrelykke, J. Chen, S. M. Mijailovich, J. P. Butler, J. J. Fredberg, and D. Stamenovic, 2002. Cell prestress. I. Stiffness and prestress are closely associated in adherent contractile cells. *American Journal of Physiology-Cell Physiology* 282:C606–C616.

3. Holle, A. W., and A. J. Engler, 2011. More than a feeling: discovering, understanding, and influencing mechanosensing pathways. *Current opinion in biotechnology* 22:648–654.

4. Wang, H.-B., M. Dembo, and Y.-L. Wang, 2000. Substrate flexibility regulates growth and apoptosis of normal but not transformed cells. *American Journal of Physiology-Cell Physiology* 279:C1345–C1350.

5. Balaban, N. Q., U. S. Schwarz, D. Riveline, P. Goichberg, G. Tzur, I. Sabanay, D. Mahalu, S. Safran, A. Bershadsky, L. Addadi, et al., 2001. Force and focal adhesion assembly: a close relationship studied using elastic micropatterned substrates. *Nature cell biology* 3:466–472.

6. Harris, A. K., P. Wild, and D. Stopak, 1980. Silicone rubber substrata: a new wrinkle in the study of cell locomotion. *Science* 208:177–179.

7. Harris, A. K., D. Stopak, and P. Wild, 1981. Fibroblast traction as a mechanism for collagen morphogenesis. *Nature* 290:249–251.

8. Sakane, A., S. Yoshizawa, M. Nishimura, Y. Tsuchiya, N. Matsushita, K. Miyake, K. Horikawa, I. Imoto, C. Mizuguchi, H. Saito, et al., 2016. Conformational plasticity of JRAB/MICAL-L2 provides "law and order" in collective cell migration. *Molecular biology of the cell* 27:3095–3108.

9. Ichikawa, T., M. Kita, T. S. Matsui, A. I. Nagasato, T. Araki, S.-H. Chiang, T. Sezaki, Y. Kimura, K. Ueda, S. Deguchi, et al., 2017. Vinexin family (SORBS) proteins play different roles in stiffness-sensing and contractile force generation. *J Cell Sci* 130:3517–3531.

10. Fujiwara, S., S. Deguchi, and T. M. Magin, 2020. Disease-associated keratin mutations reduce traction forces and compromise adhesion and collective migration. *Journal of Cell Science* 133.

11. Burton, K., and D. L. Taylor, 1997. Traction forces of cytokinesis measured with optically modified elastic substrata. *Nature* 385:450–454.

12. Li, H., D. Matsunaga, T. S. Matsui, H. Aosaki, and S. Deguchi, 2020. Image based cellular contractile force evaluation with small-world network inspired CNN: SW-UNet. *Biochemical and Biophysical Research Communications* .

13. Munevar, S., Y.-l. Wang, and M. Dembo, 2001. Traction force microscopy of migrating normal and H-ras transformed 3T3 fibroblasts. *Biophysical journal* 80:1744–1757.

14. Fukuda, S. P., T. S. Matsui, T. Ichikawa, T. Furukawa, N. Kioka, S. Fukushima, and S. Deguchi, 2017. Cellular force assay detects altered contractility caused by a nephritis-associated mutation in nonmuscle myosin IIA. *Development, growth & differentiation* 59:423–433.

15. Yokoyama, S., T. S. Matsui, and S. Deguchi, 2017. New wrinkling substrate assay reveals traction force fields of leader and follower cells undergoing collective migration. *Biochemical and biophysical research communications* 482:975–979.

16. Nehwa, F. J., T. S. Matsui, L. Honghan, D. Matsunaga, Y. Sakaguchi, and S. Deguchi, 2020. Multi-well plate cell contraction assay detects negatively correlated cellular responses to pharmacological inhibitors in contractility and migration. *Biochemical and Biophysical Research Communications* 521:527–532.

17. Watts, D. J., and S. H. Strogatz, 1998. Collective dynamics of 'small-world'networks. *nature* 393:440.

18. Neal, Z. P., 2017. How small is it? Comparing indices of small worldliness. *Network Science* 5:30–44.

19. Isola, P., J.-Y. Zhu, T. Zhou, and A. A. Efros, 2017. Image-to-Image Translation with Conditional Adversarial Networks. *CVPR* .

20. Tseng, Q., E. Duchemin-Pelletier, A. Deshiere, M. Balland, H. Guillou, O. Filhol, and M. Théry, 2012. Spatial organization of the extracellular matrix regulates cell–cell junction positioning. *Proceedings of the National Academy of Sciences* 109:1506–1511.

21. Martiel, J.-L., A. Leal, L. Kurzawa, M. Balland, I. Wang, T. Vignaud, Q. Tseng, and M. Théry, 2015. Measurement of cell traction forces with ImageJ. *In* Methods in cell biology, Elsevier, volume 125, 269–287.

22. Plotnikov, S. V., B. Sabass, U. S. Schwarz, and C. M. Waterman, 2014. High-resolution traction force microscopy. *In* Methods in cell biology, Elsevier, volume 123, 367–394.

23. Schwarz, U. S., and J. R. Soiné, 2015. Traction force microscopy on soft elastic substrates: A guide to recent computational advances. *Biochimica et Biophysica Acta (BBA)-Molecular Cell Research* 1853:3095–3104.

24. Hansen, P. C., 1998. Rank-deficient and discrete ill-posed problems: numerical aspects of linear inversion. SIAM.

25. Ronneberger, O., P. Fischer, and T. Brox, 2015. U-net: Convolutional networks for biomedical image segmentation. *In* International Conference on Medical image computing and computer-assisted intervention. Springer, 234–241.

26. Cerda, E., and L. Mahadevan, 2003. Geometry and physics of wrinkling. *Physical review letters* 90:074302.

27. Stoop, N., R. Lagrange, D. Terwagne, P. M. Reis, and J. Dunkel, 2015. Curvature-induced symmetry breaking determines elastic surface patterns. *Nature materials* 14:337–342.

28. Goodfellow, I., J. Pouget-Abadie, M. Mirza, B. Xu, D. Warde-Farley, S. Ozair, A. Courville, and Y. Bengio, 2014. Generative adversarial nets. *In* Advances in neural information processing systems. 2672–2680.

29. Li, C., and M. Wand, 2016. Precomputed real-time texture synthesis with markovian generative adversarial networks. *In* European conference on computer vision. Springer, 702–716.